

Conceptual Design of Polychromator for Thomson Scattering System in JT-60SA

Hiroshi Tojo, Takaki Hatae, Takeshi Sakuma, Takashi Hamano, Kiyoshi Itami

Japan Atomic Energy Agency, Naka, Ibaraki, Japan

(Received: 18 November 2009 / Accepted: 5 March 2010)

Significant loss in transmissivity of the fiber used for the 18 years operations in JT-60U has been discovered: thereby making optimization of the filter configuration in the polychromator in Thomson scattering system for the high performance plasmas in JT-60SA is an essential task. The loss in the optical components induced by radiation from neutrons and γ -rays in particular needs to be examined. This paper concerns the optimization of the filter configuration in the polychromator with the expected error in measurements due to the radiation damage also being estimated through comparing between fibers used in JT-60U with radiation resistant fibers.

Keywords: Thomson scattering, polychromator, neutron, JT-60SA, fiber

1. Introduction

A Thomson Scattering (TS) system is an essential diagnostics tool used to measure temporal evolution of electron temperature (T_e) and density (n_e) profiles. The TS system will not only provides data for used in evaluating energy confinement time but also data for use in understanding physical phenomena such as the MHD instability, internal transport barrier, H-mode edge pedestal and ELM activities. In addition, fusion plasma experiments have gradually resulted in increased demand for high T_e values to be measured. In JT-60SA [1], the preferred range is $T_e = 0.01 - 30$ keV. The lower bound is used when measuring runaway electrons with $T_e \sim 10$ eV [2]. The intensity of scattered with short wave length photons ($\lambda = 400 - 700$ nm) strongly depends on the accuracy of a high T_e value, however there are two notable problems that arise when analyzing the TS spectrum, one being the low transmissivity of the optical fibers in the short wavelength region (< 700 nm). Neutrons and γ -ray radiation also reduce the optical transmissivity: thereby, making estimating the neutron flux and resulting errors in the measurements essential to the forthcoming high performance regime. The other problem is optimizing the design of the polychromator. The error is sensitive to the filter configuration in the polychromator used in the detectors, thus necessitating that the wavelength range at which each of the detectors needs to measure the light be identified. Reference [3] describes how to optimize the filter configurations in a polychromator using the annealing method with the ITER edge TS system. Use of this technique enables the error to be examined with respect to T_e and best configuration to be identified.

The objectives of this paper were to optimize the filter configuration for a targeted T_e with JT-60SA plasmas and to estimate the time evolution of the measured error to be changed by the neutron and γ -ray radiation. The condition

of the fibers requiring replacement also needed identifying. Another topic concerns radiation resistant fibers being compared to normal fibers for use in the error analysis. The Numerical Aperture (NA) of the normal fibers can exceed 0.3, but the materials used in the resistant fibers limited the NA to 0.2: thereby making the analysis also important in ensuring the design of the optical system supported the collection of the many TS photons. The transmissivity measurements of the fibers in JT-60U are also provided as non-resistant fiber examples.

2. Transmissivity measurements of fibers used in JT-60U

18 years of DD plasma operation in JT-60U (1991-2008) have resulted in significant damage to the optical fibers in the TS system from the radiation. The specifications of the TS system were detailed in [2, 4]. The fibers (GS-180, made by Sumitomo Electric Industries, Ltd., core diameter: 182 μm , cladding diameter: 200 μm) are constructed pure quartz with GeO_2 -doped cladding, NA = 0.3, with a total of 102 fibers being used per bundle (channel). The total neutron rate at the first wall, where it is assumed to be basically the same as the TS optical system, was roughly estimated to be 8.7×10^{14} n/cm². The fibers-optic bundles transmit the scattered light over a hundred meters to the diagnostic room. The transmissivities of the target fiber bundles were measured using a standard light source with an integrating sphere (HR4000CG-UV-NIR, Ocean Optics, Inc.) and a fiber optic multi-channel spectrometer (HP8153A, Hewlett Packard). Note that the value of the transmissivity does not include the filling rate of the fiber bundle packing. The spectrum through the target fiber bundles was first measured, thus allowing the relative transmissivity spectrum to be estimated by using the ratio of the spectrum through the fiber bundle with that of a 2 meter long test fiber bundle. Note that apart from the length, the

2-meter-test fibers had the same specification as the 100-meter fiber. Use of the spectrometer required the incident light to be input into another fiber (P400-2-UV-VIS). However, the effective size of the fiber input was small when compared to the image size of the end section of the 100-meter-fibers, with the NA value of ~ 0.2 of the fiber also being inadequate. The error caused by any misalignment of the fibers bundles therefore relied significantly on the power measured by the spectrometer and the prevention of any of the incident light being collected. The transmissivities were therefore corrected using another measurement with a power meter that has the wider sensitive area of $\sim 6.3 \text{ mm}^2$ (referred as “power calibration”). Four narrow band-passed filters (FWHM $< 20 \text{ nm}$) at 502.4, 566.1, 599.6 and 694.6 nm were utilized. The ratio of the power of the test fiber bundle to that of the 100-meter-fiber bundles for each filter was used in precisely evaluating the transmissivities. Wide range transmissivities (400 - 1000 nm) were then finally determined using the least square method to identify the best fit between the two measurements. Figure 1 provides an example of the transmissivity spectrum of a fiber installed in 1991 and located at $z = 0.458 \text{ m}$ (vertical coordinates of the target), together with the transmissivity measured in 1991 (green). The 3 points of data recorded in 1991 confirms decreases of -1.3 dB (700 nm), -2.8 dB (600 nm) and -7.3 dB (500 nm) to have taken place. It is believed that that degradation resulted from neutron and γ -ray radiation because it is particularly severe in the short wavelength (λ) region. The noises at $\lambda < 480 \text{ nm}$ and $\lambda > 900 \text{ nm}$ was caused by lack of output intensity of integrating sphere and/or detector in the spectrometer lacking sufficient sensitivity.

3. Thomson scattering system in JT-60SA

The TS system is one of the backbone diagnostic systems used in JT-60SA. In the present conceptual design a diagnostic laser beam is injected tangentially to the toroidal direction, with three viewing fields covering entire plasma radial space area. Figure 2 presents a schematic of the viewing field of the system. Port P1 (outboard edge system), P2 (core system), and P5 (inboard edge system) cover the entire radial position. The optical systems are located in the port-plugs where no vacuum is necessary. The planned specifications are summarized in Table 1. An existing YAG laser system ($\lambda_l = 1064 \text{ nm}$) with 7.4 J (Max.) of output energy and a 50 Hz repetition rate [5] will be used as the diagnostic laser. The corrected light will be transmitted to by 100 meter long fiber to the polychromators in the diagnostic room. The polychromators consists of Avalanche Photodiode Detectors (APDs) with band-pass filters being used to acquire the appropriate wavelength regions as presented in Fig.3. The quantum efficiency of the APDs, the transmissivity of the 100 meter long fiber, and the optical components are shown in Fig. 4.

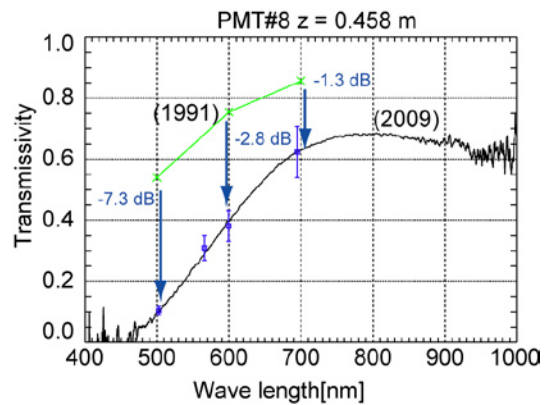


Fig. 1 Measured spectral transmissivity of a used fiber in JT-60U (PMT#8). The four blue points are the results from power calibrations. The light green line is data obtained in 1991.

As mentioned above low transmissivity can be clearly seen in the fiber data in the short wavelength region, with even further decay being expected from the severe damage caused by radiations in JT-60U experiments. Radiation resistant fiber (Mitsubishi Cable Industries, Ltd) were therefore utilized in the calculations. Decreases in transmissivity in the short wavelength region are seen from 0 C/kg to 258 C/kg (e.g. at 600 nm changed from 0.8 to 0.5). At more than 258 C/kg, however, some improvements were observed in the middle wavelength range of 600 – 900 nm (e.g. increased from 0.6 to 0.8 at 700 nm). One possibility for that recovery may be the radiation hardening that has been observed in irradiation experiments such as [6]. It is believed that impurities in the fiber tend to bond the Si and O radicals generated by the radiation thus curing the broken structures. The core diameter of the fiber is 200 μm with an NA value of 0.2 and a length of 100 m. Note that a lack of data resulted in assumption being made for the transmissivity at 0 C/kg in ensuring that the loss in dB/km had a linear relation from 420 - 500 nm. Notch filters are being planned to be used to prevent dominant line emissions being treated as background signals in the measurements. In this paper the assumption was made that filters with 20 nm of FWHM (Full Width at Half Maximum) against D_α at 656 nm, which will be the dominant line radiation, were being used. The filling rate in the fibers was also assumed to be 60 %. The transmissivity and reflection rate of each lenses and band-pass filters were considered to be 95 % with the channels being placed in the order from the shortest wavelength region to ensure that the first channel could be used to detect the strongest light.

4. Optimization of Polychromators

4.1 Photon numbers from Thomson scattering and evaluation of relative error

The error to be calculated in determining T_e and n_e can be estimated using the photon numbers from TS, bremsstrahlung, and impurity line radiation. The calculations required the following differential photon cross section provided in [7]:

$$\frac{d^2\sigma_p}{d\epsilon d\Omega_s} = q(\epsilon, \theta, 2\alpha) r_e^2 \times \quad (1)$$

$$\frac{\exp(-2\alpha\sqrt{1+\epsilon^2/(2(1+\epsilon)(1-\cos\theta))})}{2K_2(2\alpha)(1+\epsilon)^2\sqrt{\epsilon^2+2(1+\epsilon)(1-\cos\theta)}} \quad (2)$$

$$\alpha = \frac{m_e c^2}{2T_e}$$

where, $q(\epsilon, \theta, 2\alpha)$ is the depolarization factor, $\epsilon = (\lambda_s - \lambda_i)/\lambda_i$ the normalized wavelength expressed by the incident laser wavelength ($\lambda_i = 1.064 \mu\text{m}$), and scattered (λ_s) and $\Omega_s, \theta, r_e, K_2(x)$ and c are the solid angle are the scattering angle, electron radius, modified Bessel function of the second kind and the light velocity, respectively. Note that the assumption was made that the wave electric field of incident laser (E_i) being perpendicular to the scattering plane and electric field parallel to the incident would be observed. Figure 5 (top) provides the waveforms of the differential cross section, revealing the wavelength dependence on the scattered photons. It indicates at constant scattered angle ($\theta = 135^\circ$), generations of intense light with short wavelength are expected in high T_e .

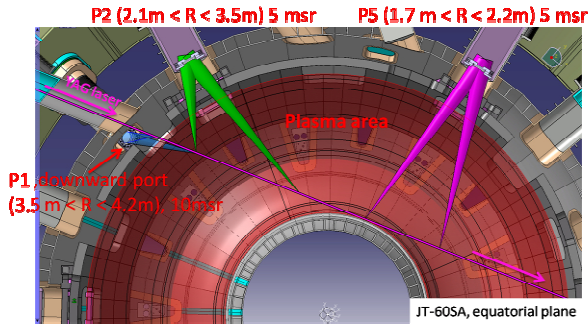


Fig. 2 Schematic of three optics from P1 (blue), P2 (green) and P5 (pink) in JT-60SA.

Table 1 Main parameters of optics system

| | P1 (outboard edge) | P2 (core) | P5 (inboard edge) |
|----------------------|--------------------------|--------------|-------------------------|
| Radial position | 0.349 0.416 m | - 0.353 m | 0.174 0.214 m |
| Scattering Length | 8 mm | 25 mm | 25 mm |

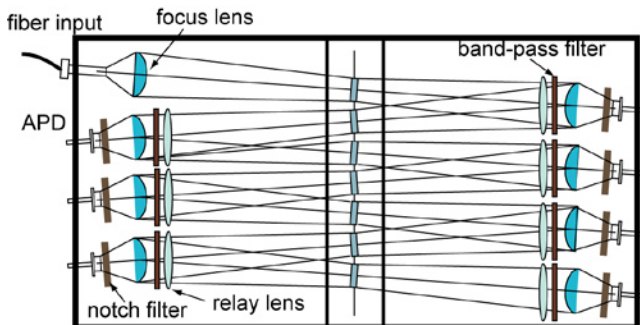


Fig. 3 Image of polychromator for JT-60SA

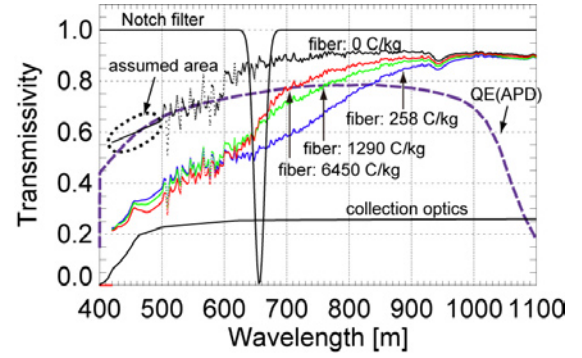


Fig. 4 Quantum efficiency of APD (dot line) and assumed transmissivity of notch filter (dashed line). Fiber transmissivity with and without γ -ray irradiation. The irradiation doses are 258 C/kg, 1290 C/kg and 6450 C/kg.

The photon numbers observed in one channel measuring the photons with $\epsilon_{j-1} < \epsilon < \epsilon_j$ can be estimated using following expression:

$$N_{s,j} = n_e \Delta L \frac{\lambda_i E_i}{hc} \Omega_s \int_{\epsilon_{j-1}}^{\epsilon_j} \frac{d^2\sigma_p}{d\epsilon d\Omega_s} \eta(\epsilon) T(\epsilon) d\epsilon \quad (3)$$

$$\equiv n_e \int_{\epsilon_{j-1}}^{\epsilon_j} S(\epsilon, \theta, 2\alpha) d\epsilon \equiv n_e g_j(T_e)$$

where j denotes the channel number, ϵ_j the boarder normalized wavelength between the wavelength region of the j th and $(j+1)$ th channels. And, $\Delta L, h, \eta(\epsilon)$ and $T(\epsilon)$ are the scattering length, Planck's constant, quantum efficiency of the APD, and the total transmissivity of the optics, including the fiber bundle, respectively. When the signal was measured, however, other photons generated by the bremsstrahlung and impurity line radiations could also be observed as background light. The back ground light in the $\epsilon_{j-1} < \epsilon < \epsilon_j$ region in particular can be written by [8], or:

$$N_{B,j} = n_e^2 \sqrt{\frac{m_e c^2}{T_e}} \frac{8}{3} \sqrt{\frac{2\pi}{3}} \frac{m_e c^2}{h} r_e^3 \Delta\Omega_s d\Delta L$$

$$\times \sin\theta D \Delta t \bar{g}_{ff} Z_{eff} \int_{\epsilon_{j-1}}^{\epsilon_j} \frac{\eta(\epsilon) T(\epsilon) K(\epsilon)}{1+\epsilon} d\epsilon \quad (4)$$

$$\equiv n_e^2 \int_{\epsilon_{j-1}}^{\epsilon_j} B(\epsilon, \theta, 2\alpha) d\epsilon \equiv n_e^2 h_j(T_e)$$

where $d, D, \Delta t, g_{ff}$ and Z_{eff} are the diameter of the incident beam, the effective pass length of the plasma, the data acquisition time (longer than the laser pulse duration), Gaunt factor, and effective ionic charge, respectively. $K(\epsilon)$ is the enhancement factor used to denote the difference resulting from theoretical estimation of the bremsstrahlung. That difference derives from the impurity lines, recombination emissions and refraction light from the wall. Note that the line integration effect is ignored in the formula, or in other words a uniform distribution (same n_e and T_e along the sight line) is assumed. $\Omega_s = 5 \text{ msr}, \theta =$

135°, $E_i = 3$ J, $\Delta L = 0.02$ m, $d = 8$ mm, $D = 2.5$ m, $\Delta t = 300$ ns, $g_{ff} = 3$, $Z_{eff} = 3.5$, $K(\epsilon) = 3$ (constant) and $n_e = 6.0 \times 10^{19}$ m⁻³ were assumed to be the parameters used in optimizations.

The photons generated by the TS are estimated by subtracting the total signal from background signal. Derivation (σ_j^2) of the measured number photons can therefore be expressed using [3], or:

$$\sigma_j^2 = N_0 + F_{noise} [n_e g_j(T_e) + 2n_e^2 h_j(T_e)] \quad (5)$$

where N_0 and F_{noise} are the dark noise and excess noise factor of the APD, respectively. In this analysis N_0 was assumed to be 225 and F_{noise} 3.0 which were expected with the detector gain of 100 provided in reference [9]. After determining T_e and n_e in the data analysis the following χ^2 is minimized in finding the best fit of the parameters.

$$\chi^2 = \sum_{j=1}^J \frac{(n_e g(T_e) - N_j)^2}{\sigma_j^2} \quad (6)$$

The associate errors in T_e and n_e can be estimated through a standard analysis [8]

$$\sigma_{T_e}^2 = \frac{\sum (g_j / \sigma_j)^2}{\sum (n_e g'_j / \sigma_j)^2 \sum (g_j / \sigma_j)^2 - [\sum (n_e g_j g'_j / \sigma_j^2)]^2} \quad (7)$$

$$\sigma_{n_e}^2 = \frac{\sum (n_e g'_j / \sigma_j)^2}{\sum (n_e g'_j / \sigma_j)^2 \sum (g_j / \sigma_j)^2 - [\sum (n_e g_j g'_j / \sigma_j^2)]^2} \quad (8)$$

,where g_j and g'_j respectively denote $g_j(T_e)$ and $\partial g_j(T_e) / \partial T_e$ and the summation takes place over $j=1 - J$. Here J denotes the number of channels in the polychromator. In the optimization σ_{T_e} / T_e ($\langle \sigma_{T_e} / T_e \rangle$) was averaged over 50 points within the range of $T_e = 0.01 - 30$ keV on logarithmic scale, the minimum value identified, and the best configuration of the filters in front of the APDs then determined in identifying the wavelength ranges of the detectors that should be measured. All the polychromator channels were considered to cover the entire wavelength range (420 – 1065.5 nm) in the calculations. The decision was therefore made to change the patterns by varying the bordering wavelength points where the detectors lie next to each other in the wavelength space. One of the detectors, however, needed to be reserved for the Rayleigh scattering calibrations at 1064 nm and hence one filter of 1063.5 – 1065.5 nm is employed in the calculations. Optimizing $\langle \sigma_{T_e} / T_e \rangle$ was executed with through use of the annealing method, which will be explained in the following section.

4.2 Simulated annealing method in optimization

The simulated annealing method can be used to identify the minimum values with problems that include many local minimum values in a multi-dimensional function [10], thus making it suitable for use in optimizing polychromator in question. The basic principle of the method is summarized in the following expression:

$$p = \exp\left(-\frac{E_2 - E_1}{T_{SA}}\right) \quad (9)$$

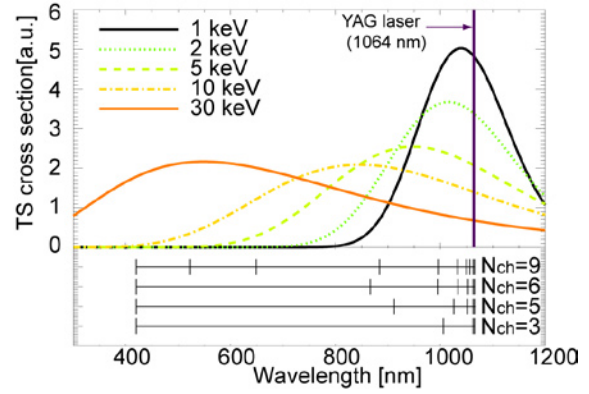


Fig. 5 (Top): Differential cross section of Thomson scattering for various T_e (1 keV – 50 keV) at $\theta = 135^\circ$. (Bottom): optimized filter configuration in the polychromator with N_{ch} values.

where E_1 and E_2 are errors defined as $\langle \sigma_{T_e} / T_e \rangle$ for each different pattern of the optical filters, p the probability that $E_2 < E_1$ and T_{SA} the constant temperature value. Use of the natural log of both sides results in the following expression:

$$E_1 = E_2 + T_{SA} \ln p \quad (10)$$

This formula indicates that some thermal noise (proportional to the temperature) is included as error in the calculations. The T_{SA} then needed to be reduced in focusing on global minimum value for E . The downhill simplex method was utilized in examining different patterned filter setup [10]. In the calculations, the T_{SA} was constantly reduced using $0.5^{(7+n)}$, where n denotes the change in the value of T_{SA} .

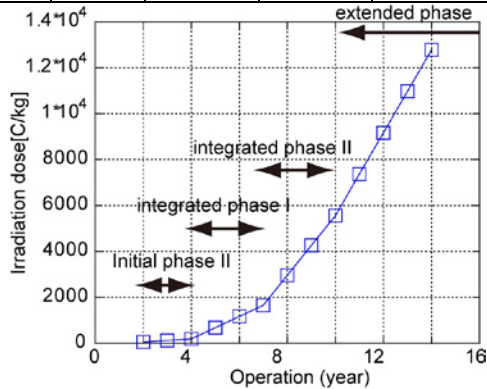
4.3 Effect from radiation and optimizations

The planned annual limitations of the neutron yield with each of the research phases and the JT-60SA are provided in Table.2. In order to assess the exposure doses resulting from neutrons and γ -rays in the fiber area of concern the neutron and γ -ray flux in the fiber position (R (major radius) = 4.7 m) were estimated utilizing 3-dimensional neutronics analysis [11]. The doses during and without the discharges were considered here. The sum of the doses estimated as C/kg and as a function of time (operational phases) is provided in Fig. 6.

As mentioned in the introduction, the fiber used in this optimization is radiation resistant. In order to estimate the transmissivity with various doses the assumption was made that 10 m would be the effective irradiated length of the 100 m fiber as the fiber bundle cables could get irradiated from the end of the collection optics to the ground floor in the machine room due to having no shielding because of the lack of space. The remaining 90 m was treated as non-damaged fiber (0 C/kg). However, and unfortunately, the exposure dose actually reaches 6450 C/kg, which is the maximum exposure dose in Fig.4 11 years after the beginning of the operations (refer to Fig. 6). This then means that at present radiation damage to the fibers could not be evaluated across all the extended phases.

Table 2 Research phases and annual neutron yields.

| | Phase | Duration (year) | Annual neutron rate | Total input power |
|------------------|-------|-----------------|----------------------|-------------------|
| Initial phase | I | 1-2y | | 23 MW |
| | II | 2-3y | 4×10^{19} | 33 MW |
| Integrated phase | I | 2-3y | 4×10^{20} | 37 MW |
| | II | > 2y | 1×10^{21} | |
| Extended phase | | >5y | 1.5×10^{21} | 41 MW |


Fig. 6 Expected time evolution of irradiation dose at $R = 4.7\text{m}$.

4.4 Optimization and time evolution of the relative error

Optimizing the filters first took place using the annealing method with different number of the detectors (N_{ch}), including one channel used in the Rayleigh calibration. The optimized patterns of the filter are revealed in Fig. 5 (at the bottom). A low average relative error was discovered at the large $N_{\text{ch}} = 6$ and that it appeared to converge at the high N_{ch} as described in Fig. 7. At a high $N_{\text{ch}} (>7)$ value the error increased because some of the APD channels were located relatively far from the input (in the high wavelength region) to the polychromator and only a small number of the photons were detected due to the reflection rate and transmissivity of the band-pass filters and lenses. The cost of the polychromators strongly depends on the N_{ch} used, making a low N_{ch} such as $N_{\text{ch}} = 5$ or $N_{\text{ch}} = 6$ more preferable. The optimized filter configurations revealed by the wavelength border of the filters were [420.0, 912.1, 1025.9, 1052.0, 1062.5, 1065.5 nm] at $N_{\text{ch}} = 5$ and [420.0, 866.2, 995.1, 1033.8, 1052.7, 1062.5, 1065.5 nm] at $N_{\text{ch}} = 6$ as revealed in Fig. 5. The dependency of the error on N_{ch} can be seen in the level of the fluctuation and the number of local minimum values provided by the waveforms. Large N_{ch} values tend to suppress any such fluctuation.

Figure 8 provides the relative error of the optimized filter configuration with respect to the T_e for various irradiated radiation resistant fibers and the fibers used in JT-60U that were treated as non-radiation resistant fibers. The damaged transmissivity shown in Fig. 1 was utilized and 0.63 assumed to be transmissivity for > 1000 nm, which is the average value within the range of 900 – 1000

nm. A less than 10 % relative error was preferable in providing information on the detailed spatial structure of physics targets such as magnetic islands. The radiation resistant fibers had a slight difference at 0 C/kg to the other irradiated fibers in the high T_e area ($T_e > 10$ keV) and which is reflected in both transmissivities in the short wavelength region. In order to clarify that difference the average relative error with respect to time (experimental phase) was evaluated, the details of which are provided in Fig.9. In that evaluation the average relative error in the range of $T_e > 10$ keV was used. The exposure dose of the fibers can be transformed into the time in years using the relationship estimated and then provided in Fig. 6. About 1% of the gradual increases in error can be seen with both $N_{\text{ch}} = 5$ and $N_{\text{ch}} = 6$, suggesting the damage caused by the radiation to be rather insignificant. However, it should be noted that the error at $N_{\text{ch}} = 5$ approaches 10 % at $T_e = 30$ keV (Fig. 8), which could result in high T_e measurements being rather difficult.

If the fiber used in JT-60U are utilized, the error is much larger than with the resistant fibers by a factor of 1.7 actually exceeding 10 % for both $N_{\text{ch}} = 5$ and 6 at $T_e = 30$ keV as revealed in Fig.8. $T_e > 10$ keV results in the 10.2 % and 8.3 % of the average relative errors being estimated for $N_{\text{ch}} = 5$ and 6, respectively. Moreover, further enhancement of the relative errors can be expected after reuse. The non-radiation resistant fiber (used fiber) therefore is inappropriate for use with such high T_e measurements.

With low T_e measurements under the condition of the assumed n_e ($6.0 \times 10^{19} \text{ m}^{-3}$) more than 10 % of the relative errors at 100 eV are inevitable even at $N_{\text{ch}} = 9$ (~ 12 %) with the radiation resistant fiber, and the determining such low T_e values for use in revealing a detailed structure of the plasma was very difficult.

5. Conclusion and future work

Optimization of the filter configuration, which depends on the transmissivity spectrum in fibers, in a polychromator was carried out. The time evolution of the relative error in T_e which was obtained by estimating exposure dose up to early on in the extended phase in JT-60SA was then evaluated. The gradual small increases in the average error (~ 1 %) in T_e was estimated for 11 years of operation, but did not exceed 10% at $N_{\text{ch}} = 6$, suggesting this number of detectors to be more suitable than $N_{\text{ch}} = 5$. With low T_e measurements more than 10 % of the relative error at 100 eV are inevitable even at $N_{\text{ch}} = 9$ (~ 12 %) at $n_e = 6.0 \times 10^{19} \text{ m}^{-3}$. Difficulties therefore are expected in attempting to understand the detailed spatial structures of a plasma with runaway electrons ($T_e \sim 10$ eV). However, that error could be reduced in high intensity discharges because a strong intensity of TS light can be expected.

Radiation resistant fiber do need to be used in high T_e values measurements (> 10 keV), otherwise a large relative errors of more than 10 % with both $N_{\text{ch}} = 5$ and $N_{\text{ch}} = 6$ could result. Note that the fibers used in the JT-60U experiments were treated as being non-resistant fiber.

Measurement of the transmissivities of the fibers used in

JT-60U revealed the significant losses to have occurred. The loss was presumably generated by the strong neutron and γ -ray radiation in the short wavelength region. Use of the resistant fiber, however, does have a disadvantage as the materials used in them limit the NA value (~ 0.2), thus requiring the size of the end face of the fiber to be enlarged. As future work the validity of Bremsstrahlung (Z_{eff}) measurements using the TS system will be discussed. In order to detect photons in a wavelength range not influenced by the line radiation in the polychromator one channel must be in the wavelength range of 1045 - 1064 nm because that range does not include the dominant line components of C, He, H, O and N (refer to Fig. 10) [12]. The uncertainty in the parameters of JT-60SA must therefore be evaluated in determining the Z_{eff} profile.

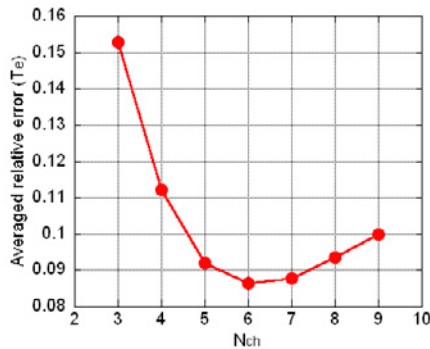


Fig. 7 Averaged relative errors in T_e with respect to the number of detectors in polychromator (N_{ch}).

6. Acknowledgements

The authors would like to express their sincere thanks to Dr. A. M. Sukegawa, Dr. E. Yatsuka, and Dr. O. Naito for their valuable discussions. Data on the fiber transmissivities was provided by the courtesy of Mitsubishi Cable Industries, Ltd.

References

- [1] T. Fujita *et al.*, Nuclear Fusion **47**, 1512 (2007).
- [2] T. Hatae *et al.*, Review of Scientific Instruments **70**, 772 (1999).
- [3] S. Kajita *et al.*, Fusion Engineering and Design **84** 2214 (2009).
- [4] H. Yoshida *et al.*, Review of Scientific Instruments **70**, 751 (1999).
- [5] T. Hatae *et al.*, Review of Scientific Instruments **77**, 10E508 (2006).
- [6] T. Shikama *et al.*, Journal of Nuclear Materials **253** 180 (1998).
- [7] O. Naito *et al.*, Physics of Fluids B **5**, 4256 (1993). (Erratum at Physics of Plasmas **1**, 806 (1994))
- [8] O. Naito *et al.*, Review of Scientific Instruments **70**, 3780 (1999).
- [9] R. Pasqualotto *et al.*, Review of Scientific Instruments **72** 1134 (2001).
- [10] W. Press *et al.*, Numerical Recipes in Fortran, second edition, Cambridge University Press (1992).
- [11] A. M. Sukegawa *et al.*, Journal of Nuclear Science and Technology, in press.
- [12] NIST Atomic Spectra Database,

(<http://physics.nist.gov/PhysRefData/ASD/index.html>.)

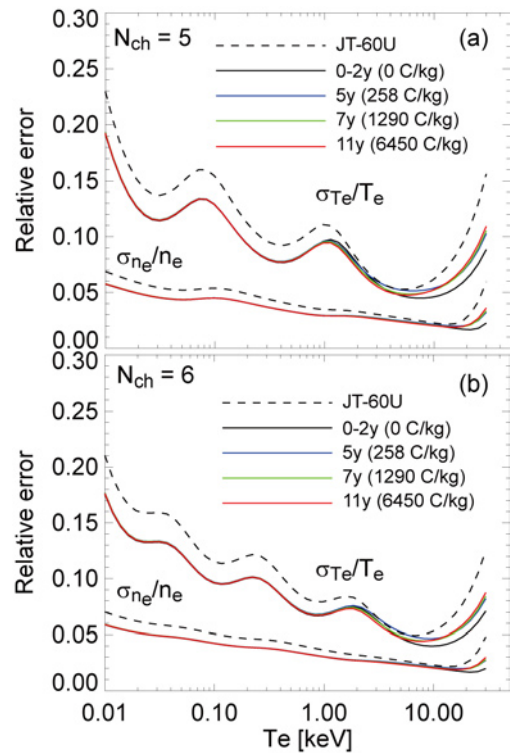


Fig. 8 Relative errors in T_e and n_e with respect to T_e at $N_{\text{ch}}=5$ (a) and $N_{\text{ch}}=6$ (b). Colors indicate different operation year (irradiation doses). Broken lines present the fiber used in JT-60U.

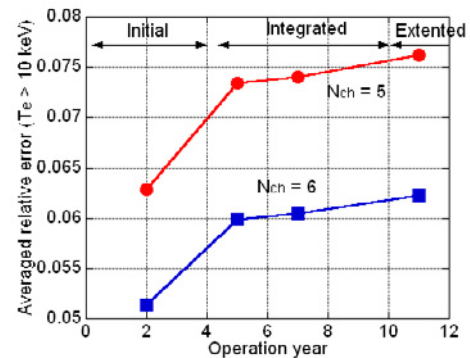


Fig. 9 Expected time evolutions of the averaged relative error in T_e at $N_{\text{ch}}=5$ (circle) and $N_{\text{ch}}=6$ (square).

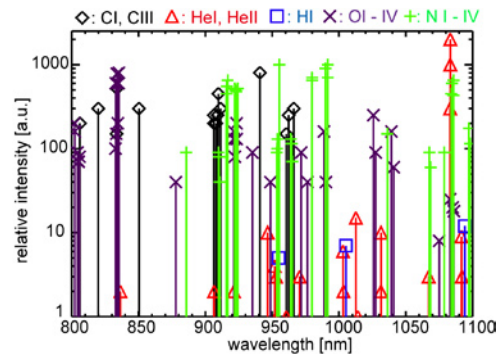


Fig. 10 The positions with line impurity emissions on wavelength space from the Ref. [12]